Journal of the European Ceramic Society **14** (1994) 67–75

X-Ray Absorption Spectroscopy Study of the Local Structure and the Chemical State of Yttrium in Polycrystalline α-Alumina

M. K. Loudjani

Laboratoire de Métallurgie Structurale, CNRS-URA 1107, Bat 413, 91405 Orsay, France

&

R. Cortès

Laboratoire de Physique des Liquides et Electrochimie, CNRS, GR4, Université Pierre et Marie Curie, 75230 Paris Cedex 05, France

(Received 15 February 1993; revised version received 10 January 1994; accepted 20 January 1994)

Abstract

The chemical state and local structure around the yttrium ion in doped polycrystalline α-alumina (0·03 ≤ mol% Y_2O_3 ≤ 1) system was examined by extended X-ray absorption fine structure (EXAFS) measurements for yttrium K-edge energy. In the case of highly doped alumina samples (0·1 and 1 mol% Y_2O_3) most of the yttrium is precipitated as a $Y_3Al_5O_{12}$ phase, whereas in the dilute doped alumina sample (0·03 mol% Y_2O_3) yttrium is in solid solution, being located on the octahedral aluminium sites. The yttrium ion size, comparatively greater than that of the aluminium ion, induces locally a significant distortion of the oxygen ion lattice. This effect creates point defects in the nearest neighbour shell of the yttrium: vacancy ($V_o^{\cdot\cdot}$) and interstitial (O_i'') oxygen point defects.

Der chemische Zustand und die lokale Struktur in der Umgebung des Yttriumions in dotiertem polykristallinem α-Aluminiumoxid (0·03 ≤ mol% Y_2O_3 ≤ 1) wurde mittels Röntgenabsorptionsfeinstrukturmessungen (EXAFS) für die Yttrium K-Kantenenergie untersucht. Bei hoher Dotierung des Aluminiumoxids (0·1 und mol% Y_2O_3) wird das meiste Yttrium als $Y_3Al_5O_{12}$ ausgeschieden, während im Falle einer geringen Dotierung (0·03 mol% Y_2O_3) Yttrium gelöst ist und in den Oktaederlücken des Aluminiums lokalisiert ist. Da das Yttriumion größer als das Aluminiumion ist, wird das Sauerstoffionengitter lokal erheblich verzerrt. Dieser Effekt führt zur Bildung von Punktdefekten in der nächsten Umgebung des Yttriums: Leerstellen ($V_O^{\cdot\cdot}$) und Zwischengitter- (O_i'') Sauerstoffpunktdefekte.

Grâce à la spectroscopie d'absorption de rayons-X (EXAFS) au seuil-K de l'yttrium, nous avons pu déterminer l'état chimique et l'environnement à courte distance autour de l'ion yttrium dans l'alumine polycristalline dopée (0·03 ≤ mol% Y_2O_3 ≤ 1. Dans le cas des échantillons fortement dopés (0·1 et 1 mol% Y_2O_3) la majeure proportion d'yttrium se trouve précipitée dans la phase $Y_3Al_5O_{12}$. Dans le cas d'échantillon faiblement dopé (0·03 mol% Y_2O_3) l'yttrium forme une solution solide, sur les sites octaédriques du sous réseau aluminium. En raison de la forte taille de l'ion yttrium, par comparaison à celle de l'ion isoélectronique aluminium, cet élément provoque des distorsions appréciables dans le sous réseau oxygène. Cet effet se traduit par la création de défauts localisés autour de l'yttrium: lacunes ($V_o^{\cdot\cdot}$) et interstitiels (O_i'') d'oxygène.

1 Introduction

The transport properties of non-stoichiometric oxides are controlled by the population of extrinsic point defects. Donor or acceptor impurities incorporated in the material can notably modify the transport properties. α-alumina with its very limited range of non-stoichiometry, can show either ionic or electronic conductivity according to the nature of the impurities and to the values of the

Journal of the European Ceramic Society 0955-2219/94/$7.00

thermodynamic parameters (T, p_{O_2}).[1-3] Point defects whose formation is promoted by a p_{O2} increase consist of aluminium vacancies V_{Al}''' and of oxygen interstitials O_i'', O_i' or O_i''. Defects whose formation is promoted by an oxygen decrease are aluminium interstitials $Al_i^{\cdot\cdot\cdot}$ and oxygen vacancies $V_O^{\cdot\cdot}$.

Much work has been performed on bulk (synthetic) α-alumina in order to understand the role of yttrium doping on the nature and the migration of the point defects in this oxide. Particular mention can be made of conductivity (σ) measurements either at thermodynamic equilibrium or in transient conditions,[1-8] or of ionic or electronic transport number determinations $t_{(i,e)} \approx \sigma_{(i,e)}/\sigma$,[2,3] or of auto/heterodiffusion measurements.[1,4,5,9,10] Such indirect techniques show that yttrium-doped alumina behaves as an ionic conductor at high oxygen pressure ($p_{O_2} \geq 10^{-4}$ atm) and as an electronic conductor at low oxygen pressure and that this behaviour is inverted for undoped alumina. This indicates that yttrium acts as a donor, an effect perhaps attributable to the great size of the yttrium ion compared to that of the aluminium ion. To date, this suggestion has not been experimentally verified.

The objective of this study consists in clarifying the role of yttrium on the point defect population by determining, using the X-ray absorption spectroscopy technique (XAS), the site in alumina on which yttrium ions are localized and the nature of the disorder created by this doping element. Such a technique reveals the local order around a doping element in a solid. From the signal provided by an EXAFS (extended X-ray absorption fine structure) experiment, it is possible to determine the R_j distance and the N_j neighbouring atom number in a given coordination shell. In addition, K-edge energy analysis, XANES (X-ray absorption near edge structure), gives information about the site symmetry and about the doping element charge.[11] Thus, polycrystalline alumina samples have been fabricated by sintering with various Y_2O_3 doping amounts, and standards of aluminium-yttrium oxides (Y_2O_3, $Y_3Al_5O_{12}$) have been prepared.

2 Experimental and Data Analysis

2.1 Experimental setup

The experimental (transmission and fluorescence) measurements were performed at room temperature at LURE-DCI (Orsay), using the EXAFS II spectrometer with a Si 311 and Si 511 double crystal monochromator. Technical details on the characteristics of the spectrometers are given elsewhere.[12] During the measurement, the synchrotron was typically operating at an energy of 1·85 GeV, with an average beam current of 300 mA. The curves are plotted over an energy range of 1000 eV by steps of 0·2 eV for XANES measurements and 2 eV for the EXAFS data collections. The yttrium K-edge is at approximately 17030 eV. In the transmission mode the EXAFS signal was recorded by measuring $I_o(E)$ and $I_t(E)$ for each energy value, with two ionization chambers. In the fluorescence mode the EXAFS signal was obtained by measuring $I_o(E)$ and $I_f(E)$ with an ionization chamber and a NaI(Tl) crystal respectively, and was the average of five scans, with five second integration times for each step.

The standard samples Y_2O_3, $Y_3Al_5O_{12}$ and the 1 mol% Y_2O_3-doped polycrystalline α-alumina were studied in the transmission mode.

The samples of 0·1 and 0·03 mol% Y_2O_3-doped polycrystalline α-alumina, after sintering, were studied in the fluorescence mode.[5,13]

2.2 Sample preparation

The transmission measurement with synchrotron radiation needs a sample thickness (x) such that $\Delta\mu.x \approx 1$–2, $\Delta\mu$ being the jump of the absorption at the K-edge.[14] Yttrium-doped polycrystalline α-alumina was obtained by hot pressing.[5] Then the specimens were annealed for 24 h in air at 1450°C. Samples of 30 × 35 mm^2 were cut and polished on the two faces up to 2-μm diamond paste until their thickness (x) was ≈ 700 μm. The standard samples Y_2O_3 and $Y_3Al_5O_{12}$ were made using submicron oxide powder;[5,15] their thickness was ≈ 170 μm.

In the fluorescence mode, the sample thickness may be higher than the depth of X-ray penetration in yttrium-doped polycrystalline α-alumina. Thus, the thickness of the specimens was chosen as ≈ 10 mm.

2.3 Data analysis

In the fluorescence mode and for the lightly doped thick sample, the fluorescence (I_f) radiation is sensitively proportional to the yttrium absorption coefficient (μ_Y), given by:[13]

$$\mu_Y \propto \frac{If}{I_O}$$

For such samples, the fluorescence intensity is very weak, making it necessary to plot a lot of spectra and to deduce the average value.

For the EXAFS analysis, the data, after conventional treatment,[16-19] were transformed using k^2 weighting and the Kaiser–Bessel window function ($w(k)$), $w(k)$ being applied over the 2·5 to 13·5 Å^{-1} range. Using single scattering theory and the

plane-wave approximation, the normalized oscillatory part of the absorption spectra is described as:[20]

$$\chi(k) = \frac{\mu_Y(k) - \mu_o(k)}{\mu_o(k)}$$

$$\chi(k) = \Sigma_j(N_j/kR_j^2)f_j(k,\pi) \exp[-2R_j/\lambda(k)] \times \exp[-2\sigma_j^2k^2] \sin[2kR_j + \phi_j(k)]$$

Where $k(\text{Å}^{-1}) = \sqrt{0{\cdot}262(E - E_0)}$ is the electron wave vector (E_0 is the yttrium K-edge energy in eV), μ_Y is the experimental absorption coefficient for the yttrium K-edge, $\mu_0(k)$ is the smooth background, $f_j(k,\pi)$ is the backscattering amplitude from each of the N_j equivalent neighbours of j type which are located at an average distance R_j from the absorbing atom, σ_j is the Debye–Waller term and $\Phi_j(k)$ is the total phase shift including central atom and backscattered contributions,[21,22] $\lambda(k)$ is the mean free path of the photoelectron. In the present case, it was considered that λ changes with k, according to the expression $\lambda(k) = k/\Gamma$, where Γ is a constant factor.[23]

In order to determine $\lambda(k)$, σ_j and ΔE_0 on the standard samples or N_j, and R_j on the doped polycrystalline α-alumina, the Fourier filtering method[16,17] was used.

The zero of the energy scale of each XANES spectrum was chosen at the yttrium energy situated at the first maximum of the derivative curve.

3 Results and Discussion

3.1 Analysis near the edge threshold (XANES)

The XANES spectra and the functions derived from the spectra obtained near the edge either by transmission or fluorescence modes for the standard samples (Y_2O_3, $Y_3Al_5O_{12}$) and for the 0·03 mol% Y_2O_3-doped alumina samples are reported in Fig. 1(a) and (b).

It appears that the threshold shape differs for the two standard compounds. Besides, from the E_0 threshold values reported in Table 1, a threshold shift ΔE between the two standard compounds can be estimated as $\Delta E = 1{\cdot}5 \pm 0{\cdot}5$ eV.

Table 1. Yttrium K-edge energy in standard samples and polycrystalline doped alumina

Samples	*Energy E_o (eV)*
0·03 mol% Y_2O_3 Polycrystalline doped alumina	17 029·5 ± 0·3
Y_2O_3 powder	17 030 ± 0·3
0·1 mol% Y_2O_3 Polycrystalline doped alumina	17 030·6 ± 0·3
1 mol% Y_2O_3, Polycrystalline doped alumina	17 031·2 ± 0·3
$Y_3Al_5O_{12}$ powder	17 031·6 ± 0·3

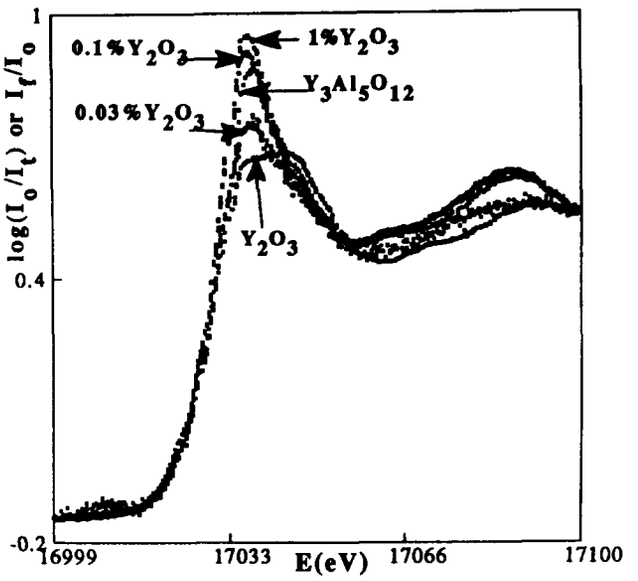

(a)

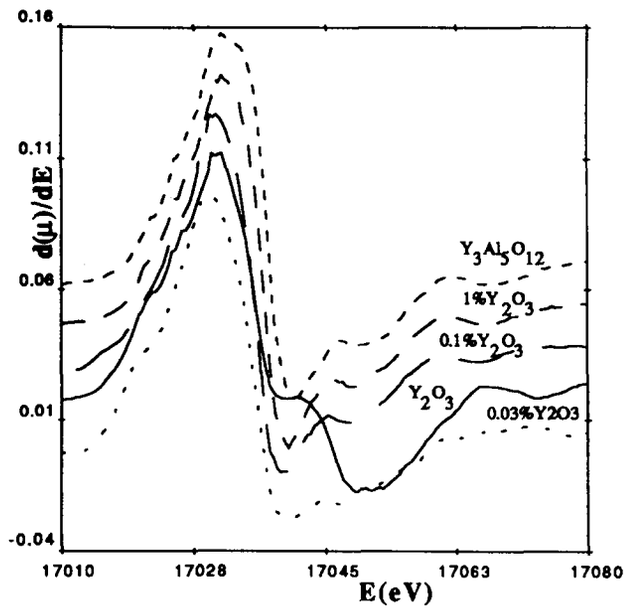

(b)

Fig. 1(a). Absorption spectra obtained near yttrium K-edge energy. (b) First derivative of the absorption spectra, for standards ($Y_3Al_5O_{12}$, Y_2O_3) and doped α-aluminas (1, 0·1 and 0·03 mol% Y_2O_3).

The threshold of the alumina samples doped with 1 or 0·1 mol% Y_2O_3 is similar to that of $Y_3Al_5O_{12}$. In contrast, the threshold of the alumina sample doped with 0·03 mol% Y_2O_3 is similar to that of Y_2O_3. Besides, in the case of the sample with the low amount of doping element, no oscillations appear after the threshold, suggesting that a partial disorder is created around the yttrium atoms.[24]

The threshold shift ΔE observed in the two standard compounds is due to the difference in the neighbouring atoms of the central yttrium atom in the two structures. Indeed, in Y_2O_3 (Ia3) the yttrium atom (types Y_1, Y_2) are surrounded on

Table 2. Theoretical distances (R_j) and number of neighbours (N_j) in $Y_3Al_5O_{12}$ and Y_2O_3 compounds

Compounds		*Shells*	*Rj(Å)*	*Nj*
Y_2O_3	Peak A	Y1–O (Y1 species)	2·249	2
		Y2–O (Y2 species)	2·261	6
		Y1–O	2·278	2
		Y1–O	2·336	2
	Peak B	Y12–Y12	3·521	3
	Peak C	Y12–Y12	3·537	3
		Y12–O	3·998	16·5
$Y_3Al_5O_{12}$	Peak A	Y–O	2·305	4
		Y–O	2·434	4
	Peak B	Y–Al1 (Al1 species)	3·003	2
		Y–A12 (A12 species)	3·357	4
	Peak C	Y–Al1	3·677	4
		Y–Y	3·677	4
		Y–O	3·876	8

average by six first neighbour oxygen atoms in octahedral coordination:[5] see Table 2. In $Y_3Al_5O_{12}$ (O_h^{10}) all the yttrium atoms are localized in pseudo-cubic symmetry sites with eight first neighbour oxygen atoms:[5] see Table 2. The differences in the crystal field created by the neighbouring atoms on the two types of yttrium sites (in Y_2O_3 and $Y_3Al_5O_{12}$) can be the origin of the threshold shift. On the derived curve related to Y_2O_3 the presence of a shoulder on the descending part of the curve is probably due to the presence of the two types of yttrium atoms (Y_1, Y_2) in 8/24 ratio. Similar shifts have been observed by fine-structure studies for transition elements (Mn, Co, Fe and Ni) in different symmetric sites.[11]

The threshold value obtained for the alumina sample doped with 0·1 mol% Y_2O_3 (as-sintered sample) is situated between the values determined for the two standard samples ($Y_3Al_5O_{12}$ and Y_2O_3), which suggests that two types of yttrium atoms are present in the 0·1 mol% Y_2O_3-doped alumina: namely yttrium atoms whose symmetry is similar to that of yttrium in $Y_3Al_5O_{12}$ and yttrium atoms whose symmetry is similar to that of yttrium in Y_2O_3.

The comparison of the energy threshold determined on Y_2O_3 and on the 0·03 mol% Y_2O_3-doped alumina suggests that yttrium ions in the lightly doped alumina sample have a coordination comparable to or slightly lower than that of the yttrium ions in Y_2O_3.

3.2 EXAFS results

3.2.1 Highly doped alumina samples (1 and 0·1 mol% Y_2O_3)

Figure 2(a) and (b) shows for the highly doped samples (1 and 0·1 mol% Y_2O_3) and for the standards ($Y_3Al_5O_{12}$ and Y_2O_3) the normalized oscillatory part of the absorption spectra and the

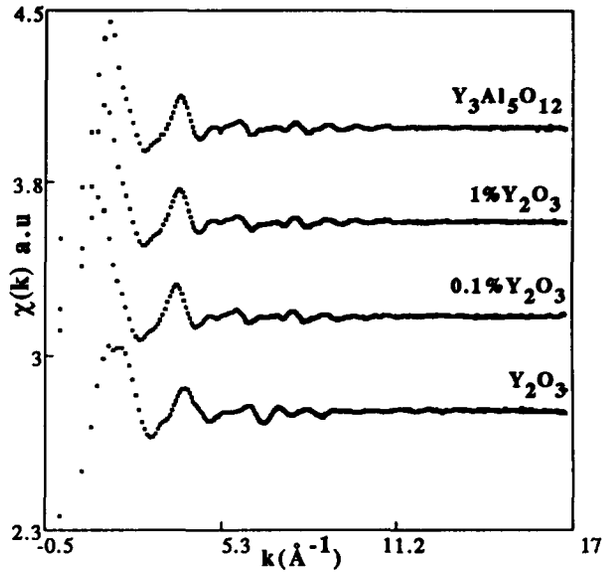

(a)

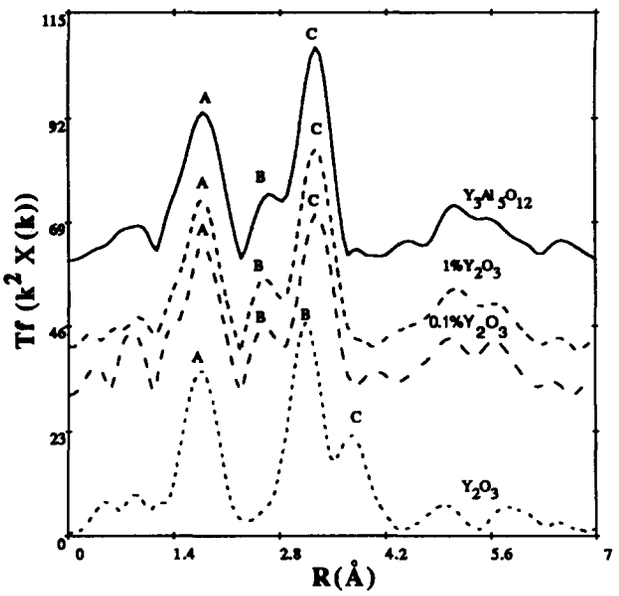

(b)

Fig. 2. (a). Normalized oscillatory part of the absorption spectra. (b) Fourier-transform magnitude spectrum (uncorrected for phase shift) of standard ($Y_3Al_5O_{12}$, Y_2O_3) and concentrated doped α-aluminas (1, 0·1 mol% Y_2O_3).

Fourier transform magnitude spectrum (uncorrected for phase shift):

$$F(r) = \int_{k_{min}}^{k_{max}} w(k)k^2\chi(k)e^{2ikr}\,\mathrm{d}(k)$$

$$k_{min} = 2{\cdot}5\text{Å},\ k_{max} = 13{\cdot}5\text{Å}$$

The $F(r)$ curve shows several peaks which correspond to the neighbouring j shells. In such a representation, these peaks are situated at distances slightly smaller than the true R_j interatomic distances, since the total phase shift $\phi j(k)$ is not considered. The true distances R_j and the number of neighbours N_j in each shell will be accurately determined when the experimental and calculated

Table 3. Fit of the parameters R(Å), N_j, determined from A, B and C peak, for the 1 and 0·1 mol% Y_2O_3 polycrystalline doped alumina (Figs 2(a) and (b))

Samples		*Shells*	$\overline{R_j(Å)} \pm 0{\cdot}01$	$\overline{N_j} \pm 0{\cdot}5$
	Peak A	⟨Y–O⟩	2·38	8·3
	Peak B	Y–Al1H	3·02	1·3
1 mol% Y_2O_3		Y–Al2H	3·70	4·9
	Peak C	Y–Al1H	3·35	3·7
		Y–Y	3·69	2·8
		⟨Y–O⟩	3·85	8·4
	Peak A	⟨Y–O⟩	2·38	7·43
	Peak B	Y–Al1H	3·03	1·9
0·1 mol% Y_2O_3		Y–Al2H	3·32	6·2
	Peak C	Y–Al1H	3·66	4·4
		Y–Y	3·71	3·2
		⟨Y–O⟩	3·90	5·2

functions ($\chi(k)_{exp}$ and $\chi(k)_{cal}$) can be fitted by taking into account the phase shift. It can be noted that the curves of the $F(r)$ pseudo-function of the radial distribution obtained either with the $Y_3Al_5O_{12}$ standard, or with the sintered samples doped with 1 or 0·1 mol% Y_2O_3, show three similar peaks A, B and C. This suggests that the neighbouring atoms around the absorber yttrium atom in the two concentrated doped alumina samples are similar to that in the garnet phase $Y_3Al_5O_{12}$. The resolution limit (ΔR_{min}) in real space related to this method[23] is given by $\Delta R_{min} \approx (3/2)\ (\pi/2K_{max})$where K_{max} is the maximum value of the wave vector in reciprocal space, i.e. $K_{max} \approx 13{\cdot}5$ Å^{-1}, and is equal to $\Delta R_{min} \approx 0{\cdot}17$ Å. It is therefore necessary, in the case of nearby coordination shells composed of atoms of similar nature, to group a given number of shells to form an average shell. The R_j radii and the N_j number of neighbours deduced from the fit in reciprocal space are reported in Table 3 for the concentrated doped alumina samples.

The shell distributions of Al, Y and O atoms around the yttrium absorber atom in the concentrated doped samples, deduced from the A, B and C peak analyses and fitting (Table 3), are similar to those of the $Y_3Al_5O_{12}$ compound (Table 2).

To summarize, the EXAFS analyses at the yttrium energy threshold indicate that in alumina samples doped with 1 or 0·1 mol% Y_2O_3, most of the absorber atoms are precipitated as $Y_3Al_5O_{12}$ (garnet phase). These results are in agreement with the thin foil observations (TEM and STEM)[5,15] concerning the $Y_3Al_5O_{12}$ precipitated phase. It must be noted that, with this method, the uncertainty on the determination of the neighbouring atom number is about 20%. Thus, it is difficult to determine accurately the stoichiometric coefficients of the precipitated phase.

EXAFS results are in agreement with the XANES study in showing that the neighbouring

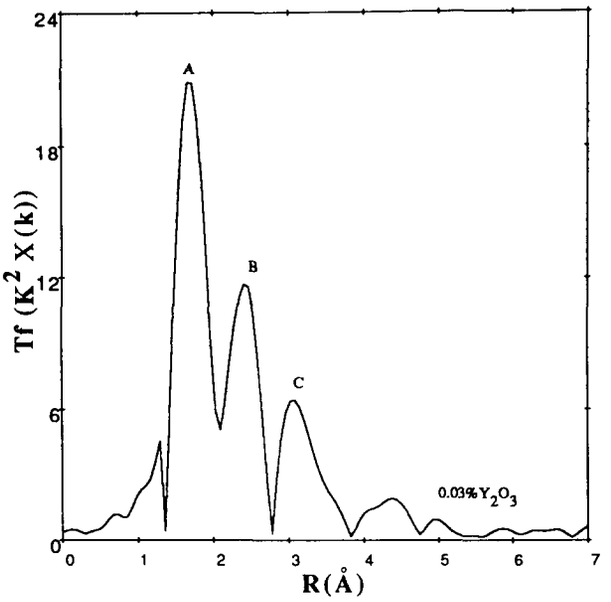

Fig. 3. Fourier-transform magnitude spectrum (uncorrected for phase shift) of dilute doped α-alumina sample (0·03 mol% Y_2O_3).

atoms around the yttrium in $Y_3Al_5O_{12}$ and in the alumina sample with a great amount of doping element (1 mol% Y_2O_3) are similar for the two structures.

3.2.2 Dilute doped polycrystalline α-alumina sample (0·03 mol% Y_2O_3)

Figure 3 shows for the dilute doped sample (0·03 mol% Y_2O_3) the Fourier transform spectrum (uncorrected for the phase shift):

$$F(r) = \int_{k_{min}}^{k_{max}} w(k)k^2\chi(k)e^{2ikr}\,\mathrm{d}(k)$$

$$k_{min} = 2{\cdot}5Å,\ k_{max} = 12{\cdot}5Å$$

The $F(r)$ spectrum (Fig. 3) does not look like the previously obtained spectra corresponding to the concentrated doped samples (Fig. 2) or to the $Y_3Al_5O_{12}$ compound. Moreover, it does not look like the Y_2O_3 and $YAlO_3$ (Perowskite-like) compounds. For $YAlO_3$, the distances and the number of neighbours are reported in Table 4 giving a calculated Fourier transform as shown in Fig. 4.

The identification of the various peaks A, B or C observed on the $F(r)$ spectrum function (Fig. 3) can be attempted by successive fitting, using as

Table 4. Theoretical distances (R_j) and neighbour numbers (N_j) in $YAlO_3$ and Al_2O_3

Samples	*Shells*	$\overline{R_j(Å)}$	$\overline{N_j}$
	Y–O	2·602	12
$YAlO_3$	Y–Al	3·187	8
	Y–Y	3·680	6
	A Y_{Al}–O	1·912	6
	B Y_{Al}–Al	2·755	4
Al_2O_3	C Y_{Al}–Al	3·403	9
	C Y_{Al}–O	3·405	9

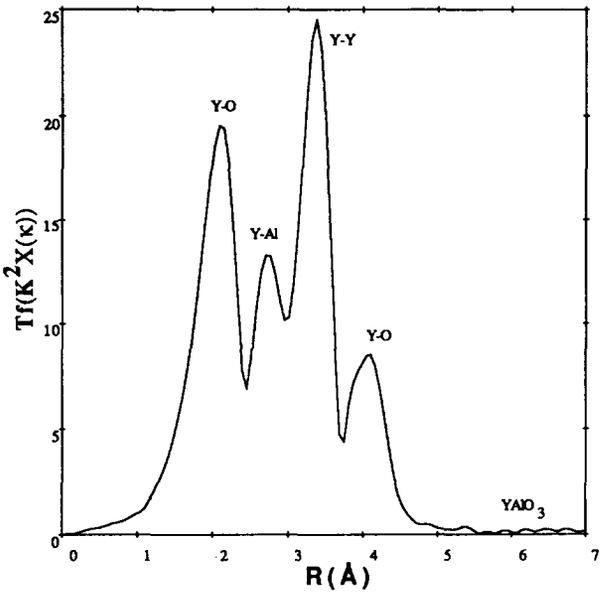

Fig. 4. Theoretical Fourier-transform magnitude (uncorrected for phase shift) calculated for ($YAlO_3$) phase.

variables the phase and amplitude functions related to the different atomic species in the sample: O, Al and Y. This analysis linked the successive peaks to the following neighbouring atoms:

- The first peak (A) corresponds to only one oxygen atom shell which includes the first neighbours of the yttrium absorber atom.
- The second peak (B) is constituted of two shells made of different atoms: Al and O.
- The third peak (C) has a small amplitude, making the determination of its composition qualitative. Nevertheless, it can be verified that the Al and O species are in a majority.

3.2.2.1 Fitting of A and B peaks. Due to the overlapping of the A and B peaks, it was necessary to take an integration window [R1, R2] in real space which brackets the two peaks. With analyses near the threshold, it was shown that the yttrium energy threshold determined on this sample is similar to that found in the standard Y_2O_3 compound (Table 2). The results of the simulation are reported in Fig. 5(a) and (b) and Table 5. It can be observed that the number of first oxygen neighbours ($N_1 \approx 2{\cdot}7$) around the yttrium is clearly smaller than in the standard Y_2O_3 or $Y_3Al_5O_{12}$ compounds in which yttrium has coordination of

Table 5. Fit of the parameters R(Å), N_j, determined from A and B peaks for the 0·03 mol% Y_2O_3 polycrystalline doped alumina (Fig. 3)

Shells	$\overline{R_j(Å)} \pm 0{\cdot}08$	$\overline{N_j}$
⟨Y–O⟩1	A 2·325	2·7 ± 0·5
⟨Y–Al⟩2	B 2·741	2·6 ± 1
⟨Y–O⟩3	B 2·845	1·7 ± 1

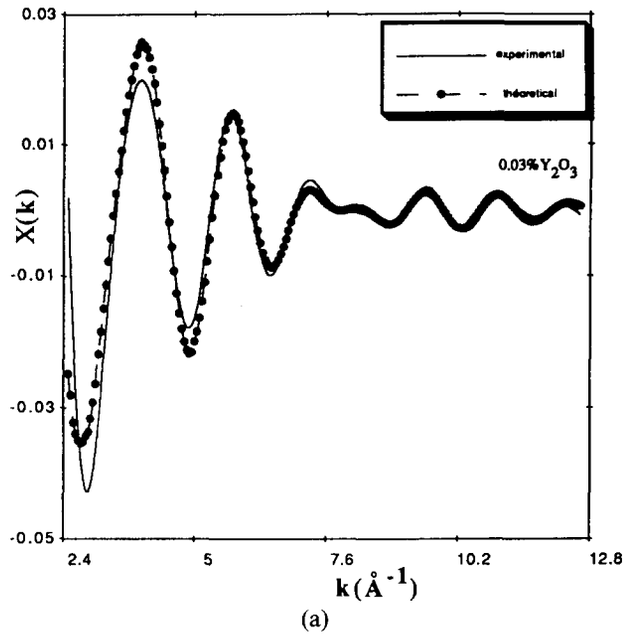

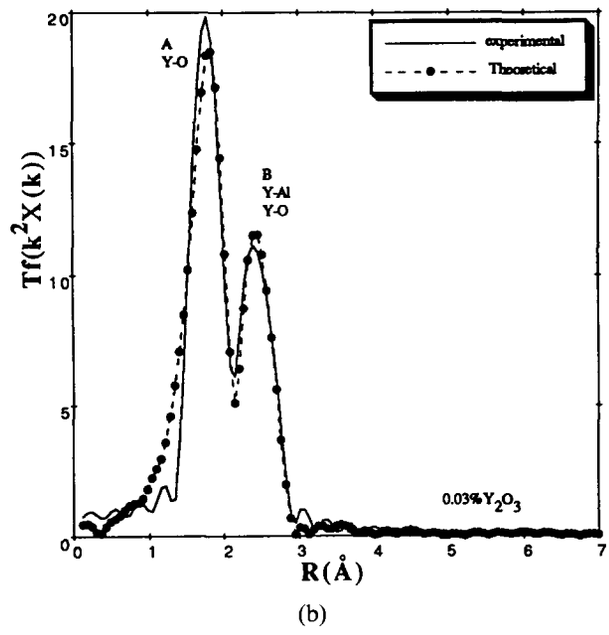

Fig. 5. Typical fitting quality in k(Å^{-1}) and R(Å) space, obtained from A and B peaks shown in Fig. 3. (a) Back-Fourier-transform spectrum ($X(k)$); (b) Fourier-transform magnitude (uncorrected for phase shift).

six and eight respectively. Assuming that the amplitude of the normalized EXAFS signal does not depend on the doping element atomic concentration, which was found to be the case for the concentrated doped samples (0·1 and 1 mol% Y_2O_3), the observed decrease of the number of neighbours can result from two factors:

—It can be due to the smoothing. Indeed, it was verified on the A peak that according to the smoothing parameter the peak amplitude can vary by about 10%.

—It can be due to the presence of oxygen vacancies $V_o^{\cdot\cdot}$ around the yttrium absorber atom.

The same analysis can be made for aluminium species. Nevertheless, due to the limited number of experimental points recorded on the B peak, this analysis is only qualitative.

The R_j distances obtained with this method are closely related to the origin of the experimental threshold. As a consequence, during the fitting of the shell related to the first oxygen neighbours, it was verified that a shift of the threshold origin from the value $\Delta E_0 = -5{\cdot}8$ (value found on the Y_2O_3 sample) to the value $\Delta E_0 = -3{\cdot}5$ eV (value found on the $Y_3Al_5O_{12}$ sample) modifies the R_j distances from 2·325 to 2·287 Å, which induces the uncertainty in Table 5.

3.2.2.2 Fitting of the C peak. On account of the small amplitude of the C peak, its fitting cannot be accurate. Nevertheless, it was found by fitting that this peak could correspond to two shells of aluminium and oxygen whose distances from the absorber yttrium atom are equal to:

$$\langle Y - Al \rangle = 3{\cdot}7 \pm 0{\cdot}5 \text{ Å}$$
$$\langle Y - O \rangle = 3{\cdot}9 \pm 0{\cdot}5 \text{ Å}$$

3.2.3 Interpretation of the results obtained with the 0·03 mol% Y_2O_3 doped sample

In order to point out accurately the site of the yttrium absorber atom in the alumina lattice, an hypothetical $F(r)$ radial distribution function was simulated (Fig. 6) corresponding to the hexagonal structure of α-Al_2O_3 in which the yttrium absorber atom is localized on an aluminium site (substitution position). In a first simulation, the difference between the size of the Al and Y species was not

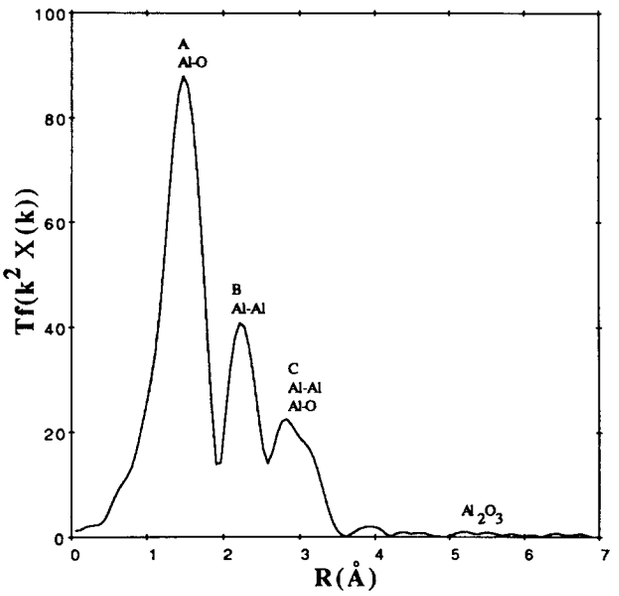

Fig. 6. Theoretical Fourier-transform magnitude (uncorrected for phase shift) calculated for (α-Al_2O_3) phase, with yttrium dissolved and located on aluminium sites, without size effect and assuming no first neighbouring yttrium ions species.

Table 6. Distances, Y–O, estimated from ionic radii, $R(Y^{3+})$ and $R(O^{2-})$, for different symmetry sites[24,25]

$R(O^{2-})$, Å	$R(Y^{3+})$, Å	
	Site VI, $R(Y^{3+}) = 0{\cdot}92$	*Site VIII,* $R(Y^{3+}) = 1{\cdot}10$
Site III, $R(O^{2-}) = 1{\cdot}28$	2·26	2·38
Site IV, $R(O^{2-}) = 1{\cdot}30$	2·28	2·40
Site VI, $R(O^{2-}) = 1{\cdot}32$	2·30	2·42
Site VIII, $R(O^{2-}) = 1{\cdot}40$	2·32	2·44

taken into account. It was assumed that there were no vacancies and that solid solution was ideal, which means that the yttrium first neighbour atoms (short distances) comprise only oxygen or aluminium species. The shell distribution of oxygen and aluminium ions, determined from crystallographic data on alumina R $\bar{3}$ c[5] is given in Table 4.

It is observed that the peak A position (Fig. 6) related to the oxygen shells obtained by such a calculation is shifted compared with the experimental A peak (Fig. 3) and that the amplitude of the calculated peak is greater. It can be noted that, on the 0·03 mol% Y_2O_3 compound, an oxygen shell (in peak B, Fig. 3) is situated at a distance from the yttrium ions equal to Y–O ≈ 2·84 Å, (see Table 5) which is not present in alumina (see Table 4). Due to this result, it can be assumed that this intermediate oxygen shell is associated with oxygen ions O_i'' in interstitial positions in yttrium 0·03 mol% Y_2O_3-doped alumina (oxygen ions removed from their usual position). This interpretation is consistent with the fact that the yttrium ions have a large size and induce an important distortion of the alumina lattice.

In order to illustrate this result, the average oxygen–yttrium distances (d = Y–O) estimated from the ionic radii of the ions Y^{3+} and O^{2-},[25,26] are reported in Table 6. According to the symmetry of the site occupied by each ion the Y–O distance varies from d = 2·26 Å for the small coordination shell to d = 2·44 Å for the larger one. The distance (2·325 Å) value of Y–O determined from the present experiments is in agreement with an yttrium site in octahedral symmetry. Thus, a new Fourier transform simulation function corresponding to the α-Al_2O_3 structure, taking into account the size effect of yttrium ions, was plotted (Fig. 7(b)). Then, a satisfactory agreement of the experimental curve (Fig. 7(a)) and of the calculated one is obtained, except for the oxygen shell situated at 2·84 Å from the yttrium ions. As the yttrium ions, localized on aluminium ion sites, are bigger ($R(Y^{3+}) \approx 0{\cdot}92$ Å than the aluminium ions $R(Al^{3+}) \approx 0{\cdot}54$ Å[24,25]) it is logical that their coordination number decreases from six to about three (2·7),

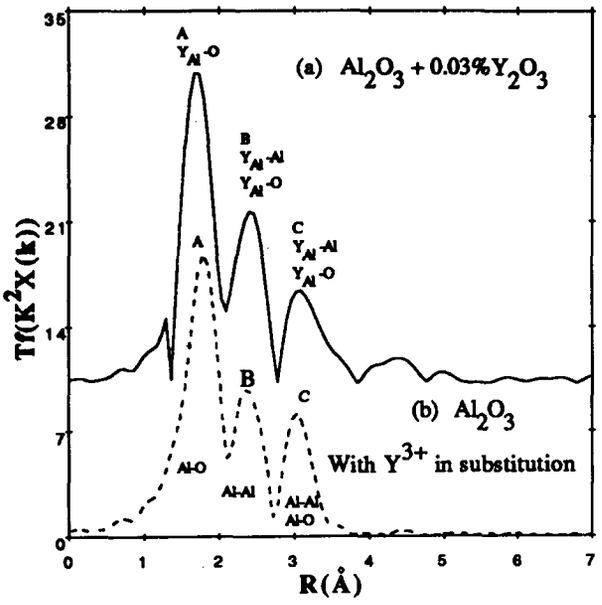

Fig. 7. (a) Experimental Fourier-transform, shown in Fig. 3 and (b) theoretical Fourier-transform magnitude calculated for (α-Al_2O_3) phase with yttrium dissolved and located on aluminium sites, taking into account the size effect of yttrium ion and the presence of vacancies in the first shell of oxygen neighbouring species.

which simultaneously induces the formation of oxygen vacancies ($V_o^{\cdot\cdot}$) and of interstitial oxygens (O_i''). This effect justifies the presence of the oxygen shell situated at 2·84 Å from the yttrium ion, oxygen shell which is attributed to oxygen ions in interstitial positions. Besides, the number of the first aluminium ion neighbours ($N_{Al} \approx 2{\cdot}6$, see Table 5) around the yttrium ions has slightly decreased, which suggests that aluminium vacancies V_{Al}''' have also been created. All these results suggest that the localized point defects around yttrium ions can be written as:

$$2Y_{Al}^{x} + 3O_o^{x} \Leftrightarrow 2Y_{Al}^{x} + 3V_o^{\cdot\cdot} + 3O_i''$$

Although the thin foil observations[5] indicate that, in this dilute doped alumina sample, a certain amount of yttrium is segregated in grain boundaries, the EXAFS signal is mainly related to the yttrium atoms localized in the bulk of the alumina grains. The experimental signal is due to the contribution of the bulk and of the grain boundaries, but this last contribution is negligible. Indeed, the grain boundary contribution is proportional to:

—The volume fraction of grain boundaries in the material, i.e. 3 δ/G (with δ and G the grain boundary width and the grain size of the material respectively).
—The relative proportion of the yttrium atomic concentration in the grain boundaries (C_j) and in the bulk (C_v), i.e. to the C_j/C_v ratio.[5]

In the present case, $\delta \approx 10$ Å,[26] $G \approx 3{\cdot}5 \times 10^4$ Å which gives 3 $\delta/G = 8{\cdot}5 \times 10^4$ and $C_j/C_v \approx 50$.[5] In such conditions, the grain boundary contribution is equal to ≈4% and can be neglected. In addition, this is confirmed by the absence of the first yttrium neighbouring atoms (Y–Y) from Fig. 3.

4 Conclusion

The XANES and EXAFS analyses at the *K*-edge of yttrium in α-alumina samples doped with various amounts of Y_2O_3 make it possible to determine the short distance order around the doping element in each case:

—In the case of highly doped alumina samples, (0·1 and 1 mol% Y_2O_3), most of the yttrium atoms are precipitated in the $Y_3Al_5O_{12}$ garnet phase. These results are in agreement with observations made by TEM on the same samples.
—In the case of the dilute doped alumina sample (0·03 mol% Y_2O_3), as sintered, the yttrium atoms do not form any definite phase such as Y_2O_3, $Y_3Al_5O_{12}$ or $YAlO_3$. The similarity between the Fourier transform function calculated by assuming that the absorber 'yttrium' atoms are localized on the aluminium sites in alumina (substitution sites) and the function determined at the yttrium threshold by EXAFS analysis indicates that most of the yttrium is dissolved in alumina and occupies aluminium sites.

Due to the size effect, the yttrium ions locally induce an important distortion of the oxygen lattice. This is structurally equivalent to the creation of oxygen vacancies ($V_o^{\cdot\cdot}$) and oxygen ions in interstitial position (O_i''). The positions of the neighbouring aluminium ions around the yttrium ions do not appear to be modified by the presence of the doping element, but their number is decreased.

Acknowledgement

The authors are indebted to P. Carry, EPFL (Lausanne), for fabricating polycrystalline aluminas and to A. M. Huntz, Orsay, for fruitful discussion.

References

1. Tiku, S. K. & Kröger, F. A., *J. Am. Ceram. Soc.*, **63**(1–2) (1980) 31.
2. El-Aiat, M. M. & Kröger, F. A., *J. Am. Ceram. Soc.*, **65**(3) (1982) 162.
3. Lee, C. H. & Kröger, F. A., *J. Am. Ceram. Soc.*, **68**(2) (1985) 71.
4. Wang, H. A. & Kröger, F. A., *J. Am. Ceram. Soc.*, **63**(11–12) (1980) 613.
5. Loudjani, M. K., Thèse de Doctorat es-Sciences, Université Paris XI, Orsay, 1992.

6. Lesage, B., Thèse de Doctorat es-Sciences, Université Paris XI, Orsay, 1984.
7. Loudjani, M., Lesage, B., Petot-Ervas, G., Deweirder, D. & Huntz, A. M., *Adv. Ceram.*, **23** (1987) 125.
8. Kitazawa, K. & Coble, R. L., *J. Am. Ceram. Soc.*, **57**(6) (1974) 250.
9. Prot, D., Thèse de Doctorat es-Sciences, Université Paris VI, 1992.
10. Le Gall, M., Thèse de Doctorat es-Sciences, Université Paris XI, Orsay, 1992.
11. Manceau, A., Gorshkov, A. I. & Drits, V. A., *Am. Min.*, **77** (1992) 1133.
12. Goulon, J., Lemonier, M., Cortès, R., Retournard, A. & Raoux, D., *Nuclear Instrument and Methods*, **208** (1983) 625.
13. Jaklevic, J., Kirby, J. A., Klein, M. P., Robertson, A. S., Brown, G. S. & Eisenberger, P., *Solid State Commun.*, **23** (1977) 679.
14. Manuel Pedro, F., Gomes Da Costa, Thèse 3ème cycle, Paris VII, 1983.
15. Loudjani, M. K., Cortès, R. Roy, J. & Huntz, A. M., *J. Am. Ceram. Soc.*, **68**(11) (1985) 559.
16. Bonnin, D., Kaiser, P., Frétigny, C. & Desbarres, J., Structure fine d'absorption X en chimie. Ecole du CNRS, Garchy, September 1988.
17. Cortès, R., Structure fine d'absorption X en chimie. Ecole du CNRS, Garchy, September 1988.
18. Kaiser, P., Thèse, Université Paris VI, 1990.
19. Kaiser, Kio, *System Analysis by Digital Computers*. Wiley, 1966.
20. Sayers, D. E., Lytle, E. W. & Stern, E. A., *Phys. Rev., Lett.*, **27** (1975) 4836.
21. Teo, B. K. & Lee, P. A., *J. Am. Chem. Soc.*, **101**(11) (1979) 2815.
22. McKale, A. G., Knap, G. S. & Chan, S. K., *Phys. Rev. B*, **33** (1986) 841.
23. Halaka, F. G., Boland, J. J. & Baldeshwieler, J. D., *J. Am. Chem. Soc.*, **106** (1984) 5408.
24. Picard-Lagnel, F., Poumelec, B. & Cortes, R., *J. Phys. Chem. Solids*, **50**(12) (1989) 1211.
25. Warren, B. E., *X-Ray Diffraction*. Addison-Wesley, Reading, MA, 1969.
26. Mistler, R. E. & Coble, R. L., *J. Appl. Phys.*, **45**(4) (1974) 1507.